Production of Dispersed Ceramic Nano-Particles in Al Alloy Using Friction Stir Processing

Amin Rabiezadeh[1*], Ahmad Afsari[2]
[1]Young Researchers and Elite Club, Shiraz Branch, Islamic Azad University, Shiraz, Iran
[2] Departments of Mechanical Engineering, Shiraz Branch, Islamic Azad University, Shiraz, Iran
*Email of Corresponding Author: rabieezadeh@iaushiraz.ac.ir
Received: October 14, 2016; Accepted: January 2, 2017

Abstract
In this research, surface composite layers containing nano sized TiB_2, Al_2O_3-TiB_2, ZrO_2 and CNT particles have been fabricated on Aluminum alloy substrates by friction stir processing. The effects of different processing variables such as number of passes and strengthening particle distribution, hardness, and wear properties of surface nanocomposite layers have been evaluated by electron microscopy, hardness, and wear test. Results showed that surface properties of aluminum alloy will be enhanced and the optimum conditions of properties which can be determined by comparing the effects of different parameters will be obtained. An increasein the number of passes up to four modifies microstructure and accordingly mechanical and wear properties were enhanced.Surface composite produced by FSP significantly improved the dry sliding wear resistance of the Al 6061 alloy by changing the wear mechanism. The FSPed sample with Al_2O_3-TiB_2 particles had higher wear resistance in comparison with those with TiB_2, ZrO_2 and CNT. This enhancement is a consequent of better bonding between particles and aluminum matrix and higher microhardness.

Keywords
Aluminum Alloy, Friction Stir Processing, Titanium Diboride, CNT, Zirconia, Wear Properties

1. Introduction

With technological progress, natural materials become insufficient to meet increasing demands on product capabilities and functions. Metal matrix composites have many advantages over monolithic metals including a higher specific modulus, higher specific strength, better properties at elevated temperatures, lower coefficients of thermal expansion and better wear resistance. Because of these attributes metal matrix composites are under consideration for a wide range of applications. For instance, metal matrix composites have attracted much attention in aerospace and aeronautical industries [1]. Uniformly dispersed reinforcements and proper interfacial bonding between the reinforcement and the matrix are the key factors to obtain excellent performance composite.

Surface properties, such as wear resistance, can determine the service life of components in many industrial applications. Components that are produced by most metals and their alloys exhibit poor mechanical and wear characteristics. Hence, there is a strong drive to develop new metal-based materials with improved mechanical and wear properties.

Low density, high strength to weight ratio, desirable physical and mechanical properties, resistance to corrosion, recovery capability and some other worthy characteristics cause aluminum and its alloys to be one of the most beneficial and desirable metals for many purposes. Nowadays aluminum and its alloys have a massive usage in military industries, aerospace, auto industries and

transport, marine industries, construction and structures and electrical industries as well. Although in some industrial usage, benefits of aluminum alloys have been limited because of lower erosion resistance and surface hardness. Al alloys the 6000 series are known to have good formability, corrosion resistance, weld ability, and high strength-to-weight ratio. They have constituted the highest volume of Al extruded products and been widely used in automobile and aerospace industries, architectural applications, bicycle frames, transportation equipment, bridge railings and welded structures. The major alloying elements in the heat-treatable 6000 series are silicon and magnesium. Both elements are required for precipitation strengthening, which is commonly acquired by solutionizing and artificial aging. Strengthening can be enhanced further by refining the grain size to a few micrometers and lower and also by compositing [2, 3].

Recently, much attention has been paid to friction stir processing (FSP), basically developed on the principle of FSW, and it is known as the surface modification technique. Similar to FSW, a rotating tool with a pin (often shorter than the thickness of the sheet) and a shoulder are inserted into a single piece of material and travel as the tool in FSW does. During FSP, the material in the processed zone undergoes intense plastic deformation, mixing and thermal exposure, resulting in significant microstructural changes. FSP has been proved to be an effective way to refine the microstructure of a material, and thereby can improve its mechanical properties. Also as shown in Figure 1, it can be used to produce surface composite layers by adding ceramic powders during the process [4-6].

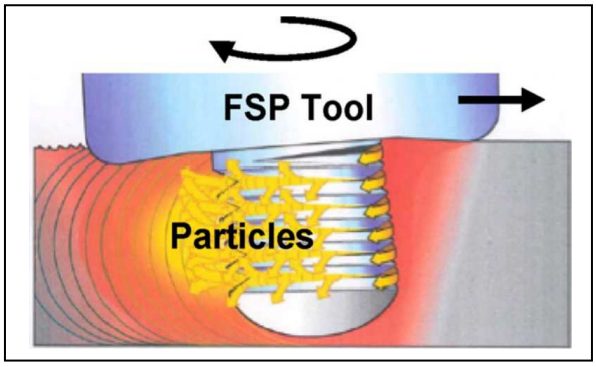

Figure1. FSP-based surface compositing process [41]

Friction stir processing is most commonly used with aluminum [7-15], but it is also used for processing other alloys, for example, Cu alloys [16-21], Zn alloys [22], steels [23-29] and Mg alloys [30-38].

Besides, friction stir processing has been used in various types of particle reinforced aluminum composite materials. Table 1 shows some of the composites made by friction stir processing.

As shown in table 1, many researchers made composites/nanocomposites by addition of ceramic reinforcement to FSP method. But till now none of them compare which reinforcements shows better mechanical or wear properties.In this study, it has been attempted to produce 6061 Al alloys matrix composites with different reinforcement phases to improve the component strength, stiffness and wear properties, using FSP. Different reinforcement phases such as TiB_2, Al_2O_3-TiB_2, CNT and

ZrO_2 were chosen due to their unique properties.Wear and mechanical properties of produced materials were compared with the as-received material and also produced nanocomposites.

Table1. Summary of the investigation on Aluminum matrix composite fabrication using FSP

Aluminum Alloy	Reinforcement	Average Particle Size	Year	Reference
AA 5083	SiC	0.7 μm	2003	[42]
AA 359	SiC	~ 10 μm	2004	[43]
AA 6061	SiC	13.4 μm	2006	[44]
AA 1050	SiC	1.25 μm	2008	[45]
5A06Al	SiC	10 μm	2009	[46]
AA 6061	SiC-Al_2O_3	300nm – 200nm	2011	[41]
AA 5052	SiC	5 μm& 50 nm	2012	[40]
AA 6061	SiC	50 nm	2012	[47]
AA 5083	SiC-MoS_2	5 μm	2012	[48]
AA 6061	SiC-Gr	20 μm	2013	[49]
AA 6082	Al_2O_3	50 nm	2009	[50]
AA 2024	Al_2O_3	50 nm	2010	[51]
AA 356	Al_2O_3	250 μm	2011	[52]
AA 5052	Al_2O_3	50 nm	2011	[53]
AA 390	Al_2O_3-Gr	~ 45 μm	2011	[54]
AA 7075	B_4C	~ 50 nm	2009	[55]
AA 6360	B_4C-TiC	~ 3 μm	2012	[56]
AA 5024	B_4C	6 μm	2013	[57]
AA 7075	TiB_2	2.62 μm	2011	[58]
AA 7075	MWCNT	Outer Dia. ~ 30-50 nm	2009	[8]
AA 5059	MWCNT	Outer Dia. ~ 30-50 nm	2012	[59]
CP Al AA 6061 AA 2009	CNT	Outer Dia. ~ 10-20 nm	2013	[60]
AA 1016	MWCNT	Outer Dia. ~ 10-40 nm	2013	[61]

2. Materials and Experimental Procedure

Aluminum 6061-T6 (T6 temper means solution treatment at 540ºC for 1h and aged at 160ºC for 12h) plates (200 mm × 70 mm × 6mm) were used as the work material. The chemical composition of the alloy is shown in Table 2. Four powders, TiB_2 (nominal diameter: 100 nm), Al_2O_3-TiB_2 (nominal diameter: 200 nm), CNT (outer diameter: 10 nm) and ZrO_2 (nominal diameter: 50 nm) were used as the reinforcements. The particle morphologies are shown in Figure 2.

Table2. Chemical composition of 6061 aluminum alloy (wt.%)

Alloy	Si	Fe	Cu	Mn	Mg	Zn	Cr	Ni	Ti	Pb	Al
6061	0.508	0.478	0.201	0.057	0.810	0.067	0.098	0.012	0.017	0.003	Bal.

The FSP tool material is made of heat-treated H13 steel; it has a shoulder of 18 mm diameter and a 3 mm long pin with a 5 mm diameter. FSP was conducted using a vertical milling machine with a constant tool rotating rate of 1600 rpm and traveling speed of 16 mm/min. To insert the powders, a groove with a depth and width of respectively 3.5 and 1 mm was machined out of work pieces, in

which the powders were filled in. Single-pass and multi-pass FSP up to four passes were carried out. In all experiments, the tool angle was fixed to 3º and the tool down force was held constant. A schematic illustration of the FSP setup is shown in Figure 3.

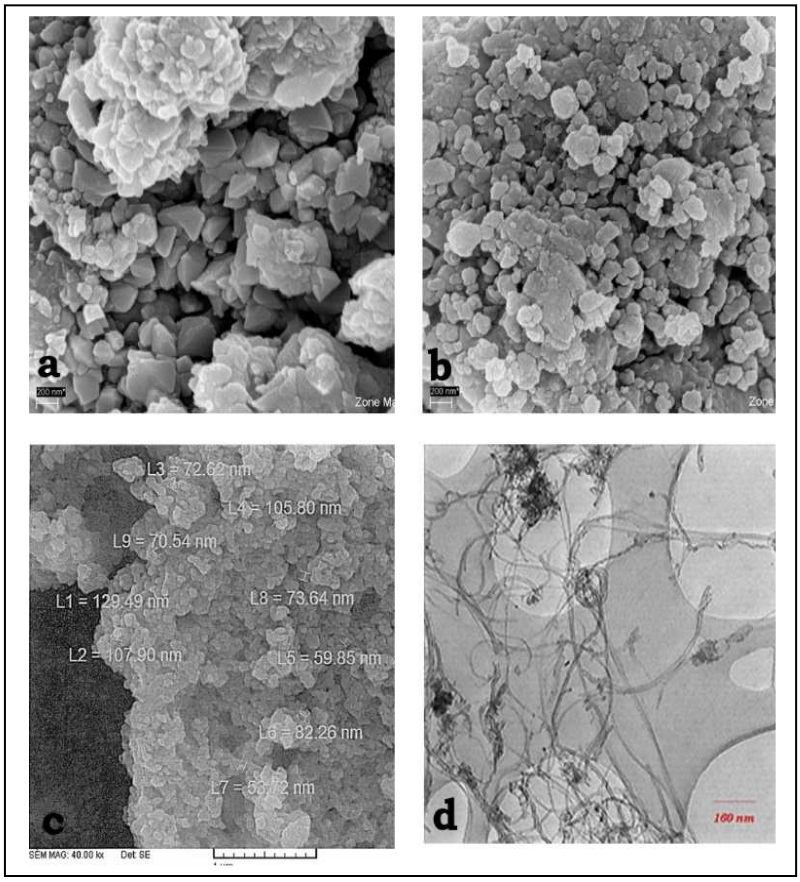

Figure2. Morphology of powders: (a) Al_2O_3-TiB_2, (b) TiB_2, (c) ZrO_2, and (d) CNT

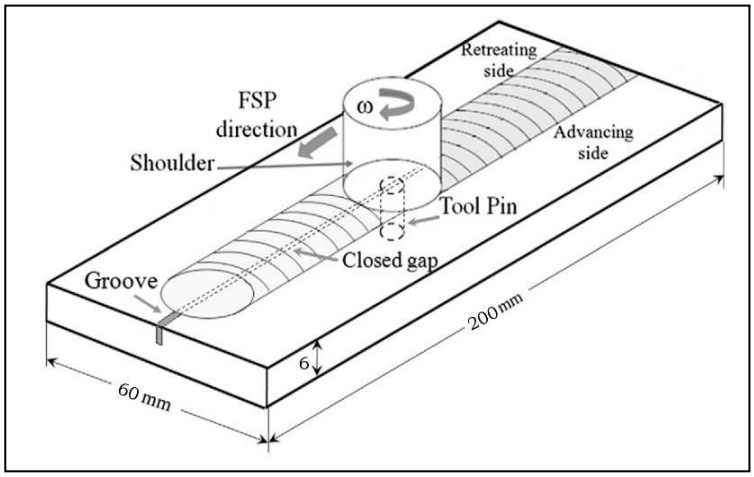

Figure3. Schematic illustration of the FSP setup

The macro and microstructural features of the FSPed regions were investigated. The FSPed samples were cut in transverse direction, then ground, polished, and examined using both optical microscope

(OM) and scanning electron microscope (SEM). Specimens were etched with Keller's reagent to reveal the macrostructure and microstructure. The size of the Al alloy grains and reinforcement particles were evaluated.

The mechanical properties of FSPed samples were measured at ambient temperature by Vickers microhardness testing and tensile testing. The microhardness indentations were made using a DHV-1000 Vickers hardness tester on metallographically prepared specimens under a load of 100 gf and for dwell time of 20 s based on ASTM E384. The mechanical properties of FSPed specimens were evaluated using universal testing machine at a constant crosshead speed of 2 mm/min based on ASTM E8. The tensile tests were performed on both the base metal and the FSPed specimens. Transverse tensile specimens were cut out from approximately the middle of the FSP plates.

The dry wear tests were conducted with a pin-on-disk apparatus based on ASTM G99. The pin specimens of 5 mm diameter were cut from the surface of as-processed specimens, with the axis of the pins perpendicular to the FSP direction. The counterpart discs were made of AISI 52100 steel with the hardness of about 60 HRc. The wear tests were carried out under dry sliding conditions for 1000m with a constant load (10 N) and a sliding velocity (0.5 m/s). Wear tests were interrupted at certain intervals to determine the progress of wear. At each interval, samples were cleaned in acetone and weighed to an accuracy of ±0.1 mg. The coefficient of friction between the pin specimen and the disk was determined by measuring the frictional force using a stress sensor.

3. Results and Discussion

Figure 4 shows the typical appearance of samples after processing. Better surface quality reduces the machinability cost required to finish the surface of the plates after FSP. According to the selected parameters, processed samples had a smooth surface and showed neither porosity nor defects. Visual evaluation, even radiographic inspection of FSPed samples didn't reveal any defects. Radiographic inspection pictures of 1, 2 and 4 passes composite samples are shown in Figure 5 which demonstrate the reliable quality of samples after processing.

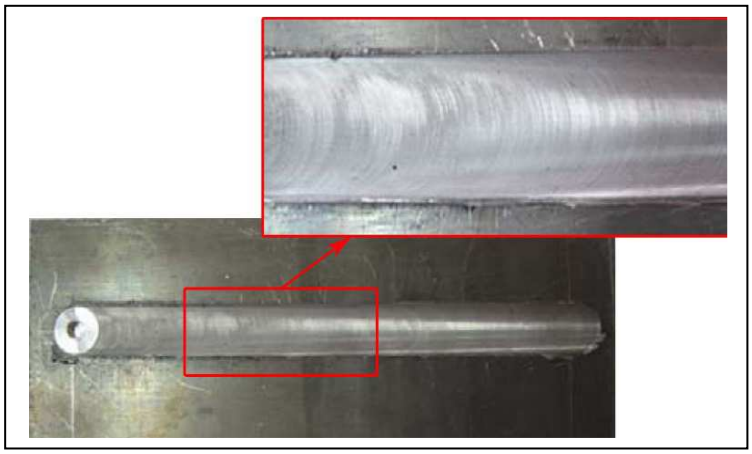

Figure4. Appearance of Al 6061/CNT sample after four passes and higher resolution (top right)

Figure 5 shows the X-ray radiography of FSPed samples. It is clearly seen that no inner defect, such as a cavity, wormhole or crack, was observed. As shown in Figures, there is no evidence of groove

after processing. Also by incrementing the number of passes, better distribution of the reinforcement particles was achieved.

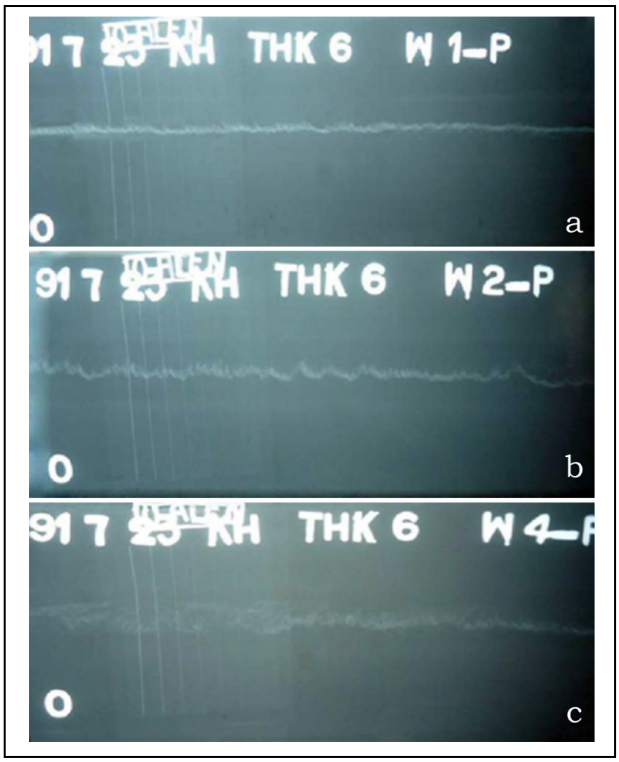

Figure5. X-ray radiography of Al 6061/ZrO_2 FSPed samples after (a) 1 pass, (b) 2 passes, and (c) 4 passes

Typical macrostructure of the friction stir processed area in the surface composite sample containing TiB_2 is shown in Figure 6, in which 4 different regions are observed. This regions include base metal (BM), friction stir zone (SZ), shoulder deformation zone (SDZ), and heat affected zone (TMAZ).

Figure6. Cross section of Al 6061/TiB_2 sample showing various microstructural zones

Figure 7 shows typical optical micrographs of the base material and stir zones of samples prepared with and without powder. The microstructure of the Al6061 base alloy is illustrated in Figure 7a. The microstructure of the as-rolled Al6061 Al alloy consists mainly of rough elongated grains with coarse Mg_2Si particles. Mean particle size of the base material is ~60µm. It is clear that the microstructure of the FSP regions is very different from that of the base alloy. The FSP zones exhibited a much more homogenous microstructure as compared to the base alloys. Within the stir zone (Figure 7b), a fine equiaxed grain structure is observed, due to the dynamic recrystallization

caused by intense plastic deformation and increase in temperature. Base material structure was destroyed and precipitates were homogeneously distributed throughout the nugget region. The stirring action of the tool during FSP resulted in breakup of Mg_2Si particles, thereby caused extensive refinement.

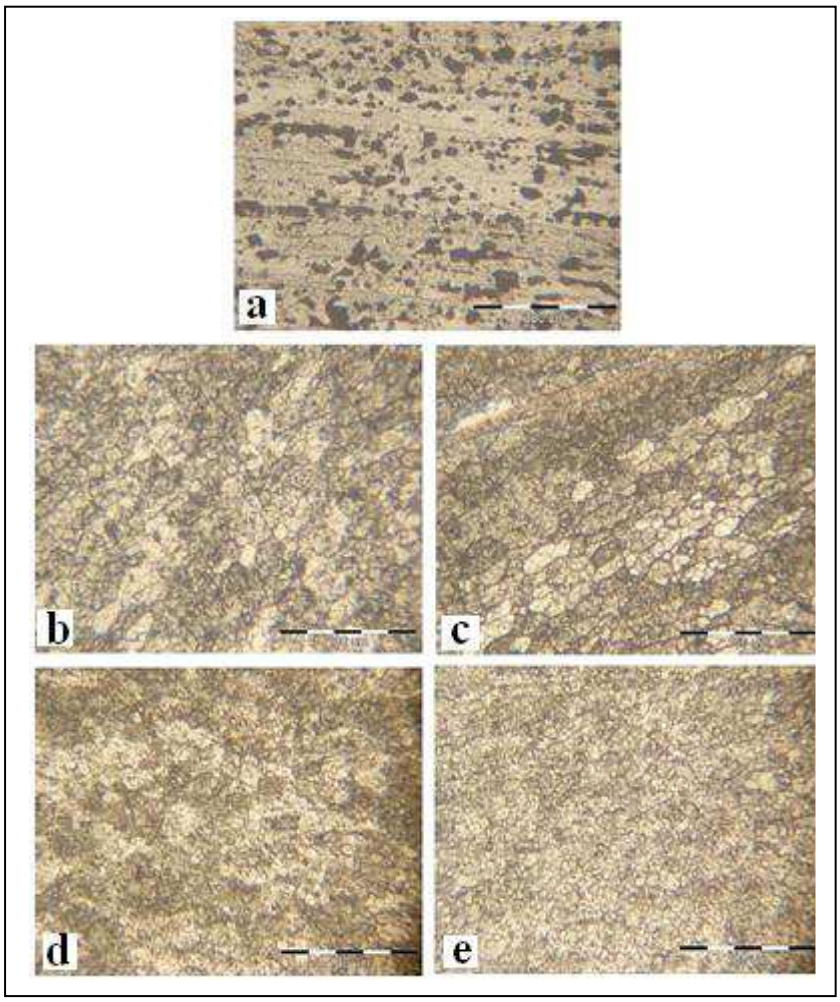

Figure7. Optical micrographs of the FSPed samples (a) base material, (b) stir zone, stir zone of Al 6061/ZrO_2 composite sample fabricated by (c) 1 pass FSP, (d) 2 passes FSP, and (e) 4 passes FSP

Figure 7c-e shows microstructure of stir zones in composite samples produced by one to four passes respectively. They are composed of fine equiaxed recrystallized grains. As can be seen, the grains of 6061 Al matrix were obviously refined by the FSP and average grain size of the stir zone decreased with an increase in the number of FSP pass. As reported by other researchers, severe plastic deformation and heat input produce fine equiaxed grains bydynamic recrystallization [10].
Dynamic recovery (DRV) occurs during hot working of metals and alloys of high stacking fault energy such as aluminum and 6061-T6 aluminum alloy. The flow stress rises during the initial stage of deformation as dislocations multiply and interact. However, the rate of recovery also increases as the dislocation density increases and dislocations begin to rearrange and form low-angle boundaries as subgrains develop. Eventually, the flow stress saturates as hardening, due to dislocation

rearrangement, reaches a dynamic equilibrium. This leads to deformation at a steady state wherein the flow stress remains constant with strain. The steady state is reflected in equiaxed subgrains with nearly dislocation-free interiors, constant subgrain size and subgrain boundary misorientation. The steady state appears to reflect continual processes of subgrain boundary formation, rearrangement, and dissolution during deformation. DRV reflects the ease of climb and cross-slip in materials of high stacking fault energy; thus, corresponding deformation microstructures tend to be homogeneous, and the absence of local strain concentrations apparently precludes alternative restoration mechanisms [10].

Therefore, the grain size of the stir zone decreased with an increase in the number of FSP pass which is due to the higher strain extruded by higher passes. Also, higher passes caused formation of grains with high density of dislocations and inhibited the growth of recrystallized grains. However, the multiple pass FSP with the nano-sized particles more effectively reduced the grain size of the 6061Al matrix.

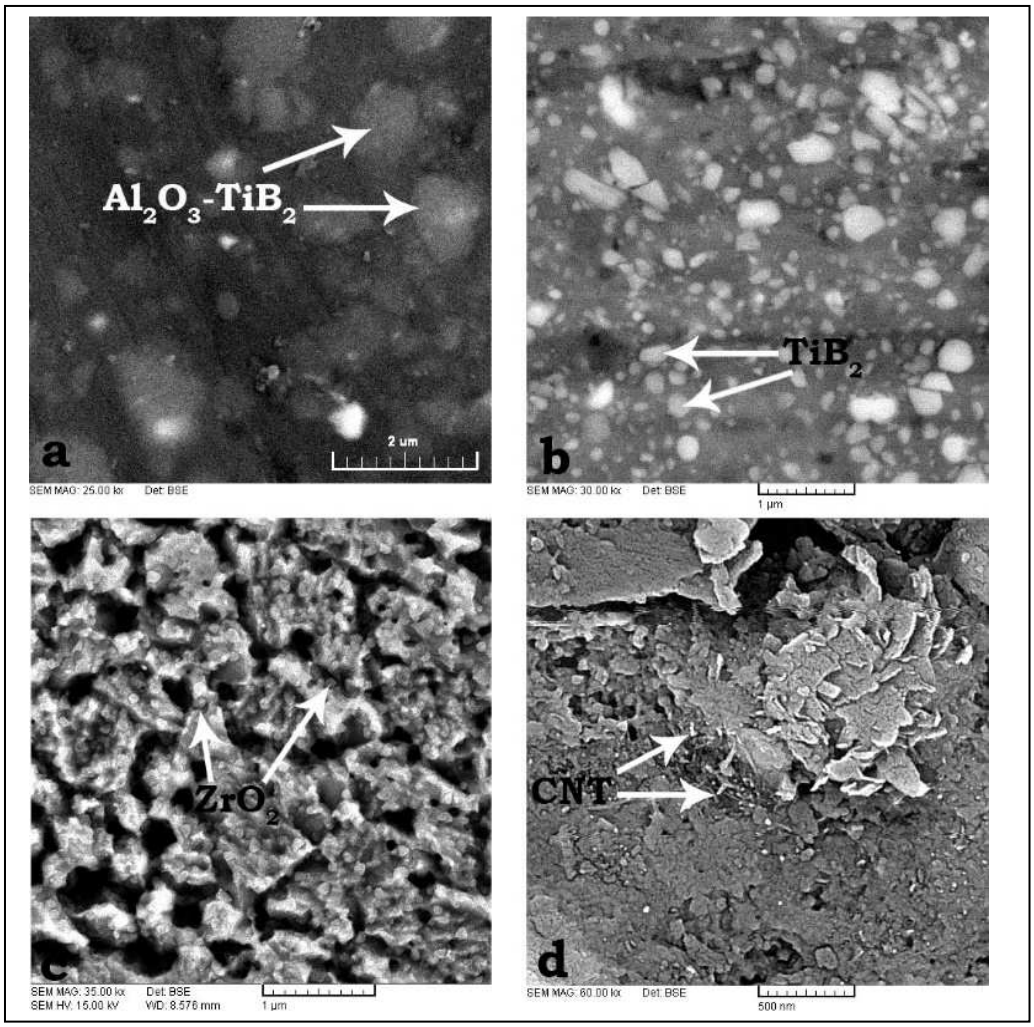

Figure8. SEM micrograph of composite samples produced by FSP with different reinforcement after 4 passes (a) Al 6061/Al_2O_3-TiB_2, (b) Al 6061/TiB_2, (c) Al 6061/ZrO_2, and (d) Al 6061/CNT

Due to the nano-size of reinforcement particles, distribution of particles in the structure is not detectable in the optical micrographs. In order to determine the distribution of reinforcement particles in the microstructure, SEM micrographs of composites were shown in Figure 8. Each micrograph revealed and a uniform distribution of reinforcement particles is in the Al matrix. A comparison of Figure 2a and b with Figure 8a and 8b shows that FSP leads to a little decrease in reinforcement particle size.

Table 3compares the Vickers microhardness of the Al 6061 alloy with different reinforcement. Vickers microhardness of as received Al 6061 and that of FSPed without particles were respectively about 95 HV and 56 HV. The FSP surface without particles is softer than the original material because of the FSP annealing effect.

Table3. Maximum microhardness attained after FSP by different reinforcement at each passes

No. of Pass\Reinforcement	ZrO_2	TiB_2	CNT	Al_2O_3-TiB_2
1	122	156	160	158
2	146	172	168	179
4	160	203	198	210

The microhardness distribution across the stir zone region is indicated in Figure 9 for the 4 passes FSPed samples with different reinforcements. The hardness profiles show significant decrease for the FSPed sample with no powder. According to Hall-Petch relationship, with a decrease in grain size, hardness value increases. On the other hand, the rise of temperature during FSP anneals material in the stirred zone. Annealing will decrease density of dislocations, residual compressive stresses of initially rolled sheets, and dissolution of precipitates. Here, the effect of annealing dominates grain refinement. Woo et al. showed that the dissolution of the precipitates during FSP causes microstructural softening, because the strength of 6xxx aluminum alloys critically depends on the density of the precipitate [39].

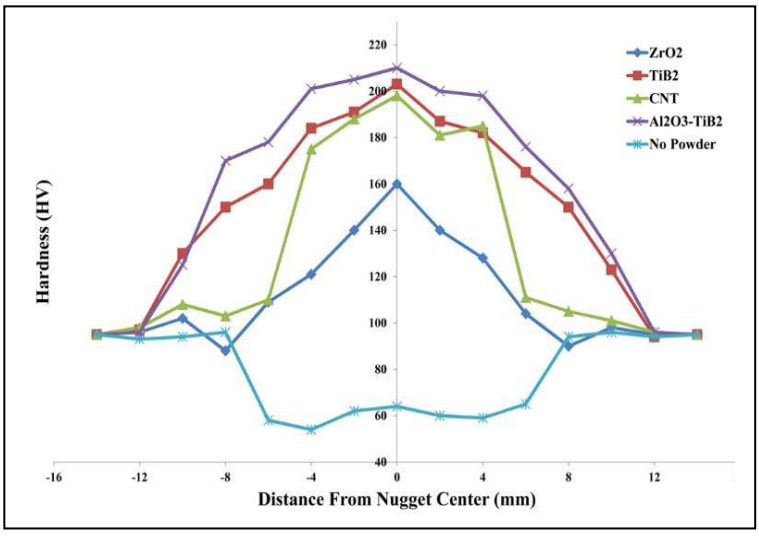

Figure9. Hardness profile of composite samples with different reinforcement after 4 passes FSP

In composite FSPed samples, three factors are involved in hardness enhancement: grain size reduction, presence of reinforcing particles in aluminum matrix, and quench hardening effect due to difference in thermal contraction coefficient of aluminum matrix and particles [40].Among the reinforcing particles, CNT is the hardest and zirconia the softest of them all. Another factor that affected on the hardness of FSPed samples was the size of reinforcing particles. Based on the experiment results that were shown in the Figure 9, 4 passes Al6061/Al_2O_3-TiB_2 was the hardest and 4 passes Al6061/ZrO_2 is the softest one.

Typical variation of friction coefficient in sliding distance of 1000m for as-received and composite samples with zirconia as reinforcement particle are displayed in Figure 10. In early stages of the test, in all samples, the friction coefficient increased to a maximum, followed by a lower steady state value. The initial increase in the friction coefficient may be due to the increase in the friction force needed to overcome the highly adhesive contact between the ball and the tested surface. The large fluctuation of the friction coefficient which was observed in all the curves presented in Figure 10 may be attributed to the periodical accumulation and elimination of wear debris on the worn track.

Friction coefficients of as received Al 6061 and FSPed samples without any particle are 0.85 and 0.72, respectively. Also, hardness enhancement with the production of composite layer positively affects wear behavior.

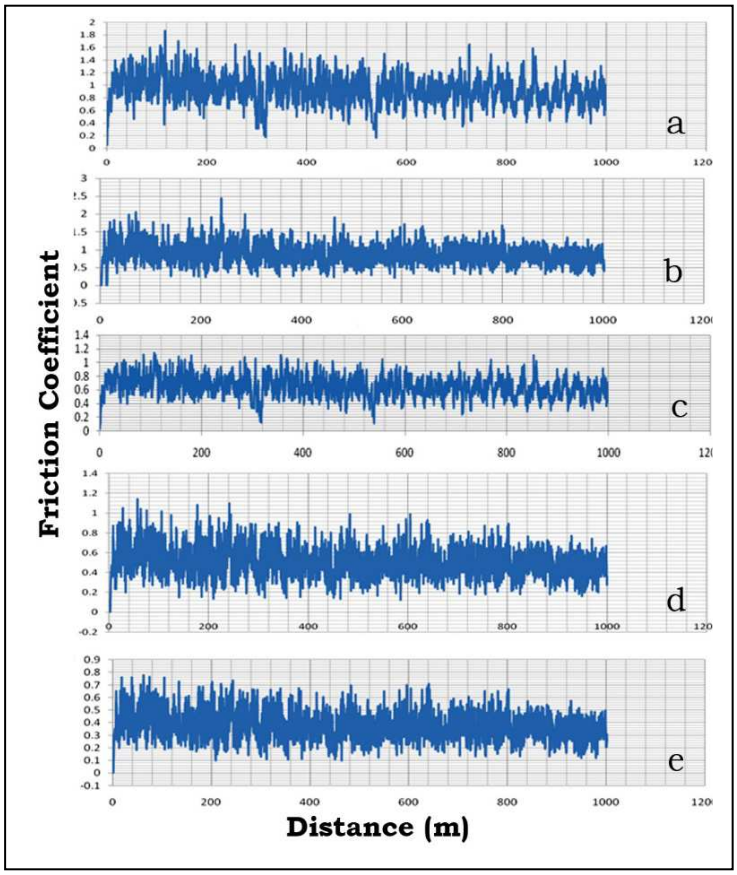

Figure10. Typical friction test data (a) Al 6061(base metal); (b) Al 6061, 1 pass FSP; (c) Al 6061/ZrO_2, 1 pass FSP: (d) Al 6061/ZrO_2, 2 passes FSP; and (d) Al 6061/ZrO_2, 4 passes FSP

Figure 10 shows that fabrication of composite layer decreases average friction coefficient, hence improvements in wear resistance. Reinforcing ZrO_2 particles in composite layer sustains wearing loads and impedes direct load contact of aluminum matrix and disk. Also, hardness enhancement with production of composite layer positively affects wear behavior. Figure 10 shows that specimen with four passes of FSP has better friction coefficient and wear behavior than specimen with one pass. Decrease of grain size, increase of hardness and better dispersion of reinforcement particles in composite layer with further passes improves wear properties.

Table 4shows the friction coefficient of all composite samples. The sample with Al_2O_3-TiB_2 particles has a higher wear resistance in comparison with those with TiB_2, ZrO_2 and CNT. This enhancement in wear properties is a consequence of better bonding between Al_2O_3-TiB_2 particles and aluminum matrix and of higher microhardness values.

Table4. Friction coefficient of composite samples produced by FSP by different reinforcement at each passes

No. of Pass\Reinforcement	ZrO_2	TiB_2	CNT	Al_2O_3-TiB_2
1	0.65	0.60	0.62	0.56
2	0.51	0.48	0.53	0.45
4	0.38	0.35	0.42	0.29

Figure 11 shows SEM micrographs of the worn surfaces for both Al 6061 and Al 6061/Al_2O_3-TiB_2 hybrid composite produced by 4 passes FSP after 1000 m of dry sliding wear. It is clear from Figure 11a and b that the worn surface of the base metal (Al 6061) specimen is rougher than the FSPed sample. The base metal specimen exhibited larger wear traces on the worn surface when compared with the worn surface of the FSPed specimen. Moreover, long ploughing lines could be seen in the worn surface of both the base metal and FSPed samples. However, more surface damage can be detected on the surface of the base metal sample. In both samples, the occurrence of extensive plastic deformation during wear is clearly observed. From Figure 11a, it is clear that an extensive surface damage due to the high material removal (delamination process) rate takes place in the base material. The composite surfaces yielded more stable and a significantly lower steady-state friction coefficient than those of the as-received base material.

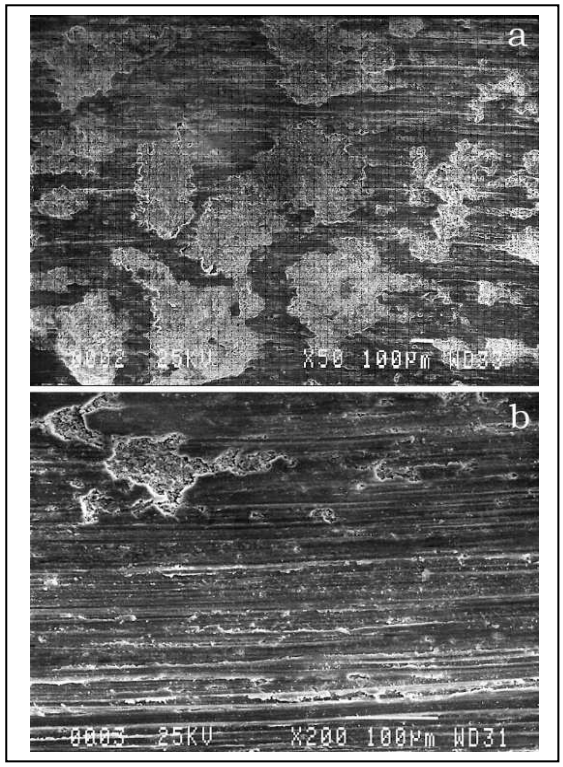

Figure11. SEM micrograph of the worn surfaces of (a) Al 6061; and (b) Al 6061/Al_2O_3-TiB_2 hybrid composite produced by 4 passes FSP after sliding distance of 1000m

More encouraging, the introduction of particles reduced the friction coefficient. It is known that adhesion dominates the sliding wear for conventional aluminum alloys, as shown by the wear scar on the Al 6061 in Figure 11a. In contrast, the worn composite surface (Figure 11b) shows much less severe adhesive wear but instead is dominated by abrasive wear and plastic deformation.
This reveals an intensive material removal and plastic deformation which proves that an adhesive wear has occurred. Besides, those deep grooves, which are signs of abrasive wear, can be observed.
The presence of reinforcing particles in specimens FSPed with reinforcement particles prevents adhesive wearing and drastic material removal. The debris particles in Figure 11b are related to oxidation and removal of base aluminum and segregation of Al_2O_3-TiB_2 particles from composite layer during wear test, so abrasive wear is the dominant wear mechanism in specimens equipped with surface composite layer. This change of wear mode is critical for achieving a significant improvement in the wear performance for aluminum-based materials.

4. Conclusions

Multi-pass FSP with different reinforcement particles was carried out on 6061 aluminum alloy to study the effects of strengthening particles on wear properties of nano-composite layers. Four types of ceramic nano-particles, TiB_2 (nominal diameter: 100 nm), Al_2O_3-TiB_2 (nominal diameter: 200 nm), CNT (outer diameter: 10 nm) and ZrO_2 (nominal diameter: 50 nm) were used as the reinforcements. Each composite material system demonstrated promising mechanical and wear properties. The following can be concluded:

- A reduction in microhardness of FSPed samples without any particles occurred due to the precipitate dissolution by the thermal cycle of FSP.
- The ultrafine grain formed during FSP and the strong interface between reinforcement particles and aluminum matrix were beneficial to the improvement of the wear properties of composites.
- An increase in the number of passes up to four led to a proper modification of the microstructure and a subsequent enhancement in mechanical and wear properties.
- Surface composite produced by FSP significantly improved the dry sliding wear resistance of the Al 6061 alloy.
- The FSPed sample with Al_2O_3-TiB_2 particles had higher wear resistance in comparison with those with TiB_2, ZrO_2, and CNT. This enhancement is a consequence of better bonding between particles and aluminum matrix and higher microhardness.

5. Acknowledgments

The authors would like to acknowledge the funding provided by Islamic Azad University of Shiraz.

6. References

[1] Rosso, M. 2006. Ceramic and Metal Matrix Composites: Routes and Properties. Journal of Materials Processing Technology. 175: 364-375.

[2] Lucas, G. 1996. Aluminum Structural Application. Advanced Materials and Processing. 149: 29-30.

[3] Barbosa, C., et al. 2006. A Microstructural Study of Flash Welded and Aged 6061 and 6013 Aluminum Alloys. Materials Characterization. 57: 187-192.

[4] Arora, H.S., Singh, H. and Dhindaw, B.K. 2012. Composite Fabrication Using Friction Stir Processing: A Review. International Journal of Advanced Manufacturing Technology. 61: 1043-1055.

[5] Ma, Z.Y. 2008. Friction Stir Processing Technology: A Review. Metallurgical and Materials Transactions A. 39A: 642-658.

[6] Besharati Givi, M.K. and Asadi, P. 2014. Advances in Friction Stir Welding and Processing. London: Woodhead Publishing, Elsevier.

[7] Ma, Z.Y. and Liu, F.C. 2008. Achieving Exceptionally High Superplasticity at High Strain Rates in a Micrograined Al-Mg-Sc Alloy Produced by Friction Stir Processing. Scripta Materialia. 59: 882-885.

[8] Lim, D.K., Shibayanagi, T. and Gerlich, A.P. 2009. Synthesis of Multi-Walled CNT Reinforced Aluminium Alloy Composite Via Friction Stir Processing. Materials Science and Engineering A. 507: 194-199.

[9] Ma, Z.Y., Sharma, S.R. and Mishra, R.S. 2006. Effect of Multiple-Pass Friction Stir Processing on Microstructure and Tensile Properties of a Cast Aluminum-Silicon Alloy. Scripta Materialia. 54: 1623-1626.

[10] McNelley, T.R., Swaminathan, S. and Su, J.Q. 2008. Recrystallization Mechanisms During Friction Stir Welding/Processing of Aluminum Alloys. Scripta Materialia. 58: 349-354.

[11] Yadav, D. and Bauri, R. 2012. Effect of Friction Stir Processing on Microstructure and Mechanical Properties of Aluminium. Materials Science and Engineering A. 539: 85-92.

[12] Feng, X., Liu, H. and Babu, S.S. 2011. Effect of Grain Size Refinement and Precipitation Reactions on Strengthening in Friction Stir Processed Al-Cu Alloys. Scripta Materialia. 65: 1057-1060.

[13] Surekha, K., Murty, B.S. and Prasad Rao, K. 2009. Effect of Process Parameters on the Corrosion Behaviour of Friction Stir Processed AA2219 Aluminum Alloy. Solid State Sciences. 11: 907-917.

[14] Alidokht, S.A., et al. 2012. Evaluation of Microstructure and Wear Behavior of Friction Stir Processed Cast Aluminum Alloy. Materials Characterization. 63: 90-97.

[15] Su, J.Q., Nelson, T.W. and Sterling, C.J. 2005. Friction Stir Processing of Large-Area Bulk UFG Aluminum Alloys. Scripta Materialia. 52: 135-140.

[16] Su, J.Q., et al. 2011. Development of Nanocrystalline Structure in Cu During Friction Stir Processing (FSP). Materials Science and Engineering A. 528: 5458-5464.

[17] Xue, P., Xiao, B.L. and Ma, Z.Y. 2012. High Tensile Ductility Via Enhanced Strain Hardening in Ultrafine-Grained Cu. Materials Science and Engineering A. 532: 106-110.

[18] Barmouz, M., et al. 2011. Investigation of Mechanical Properties of Cu/SiC Composite Fabricated by FSP: Effect of SiC Particles' Size and Volume Fraction. Materials Science and Engineering A. 528: 1740-1749.

[19] Surekha, K. and Els-Botes, A. 2011. Development of High Strength, High Conductivity Sopper by Friction Stir Processing. Materials and Design. 911-916: 32.

[20] Barmouz, M., Besharati Givi, M.K. and Seyfi, J. 2011. On the Role of Processing Parameters in Producing Cu/SiC Metal Matrix Composites Via Friction Stir Processing- Investigating Microstructure, Microhardness, Wear and Tensile Behavior. Materials Characterization. 62: 108-117.

[21] Xue, P., Xiao, B.L. and Ma, Z.Y. 2013. Achieving Large-Area Bulk Ultrafine Grained Cu via Submerged Multiple-Pass Friction Stir Processing. Journal of the Materials Science and Technology. 29: 1111-1115.

[22] Hirata, T., et al. 2007. Relationship Between Deformation Behavior and Microstructural Evolution of Friction Stir Processed Zn–22 wt.% Al Alloy. Scripta Materrialia. 56: 477-480.

[23] Aldajah, S.H., et al. 2009. Effect of Friction Stir Processing on the Tribological Performance of High Carbon Steel. Wear. 267: 350-355.

[24] Chabok, A. and Dehghani, K. 2010. Formation of Nanograin in IF Steels by Friction Stir Processing. Materials Science and Engineering A. 528: 309-313.

[25] Noh, S., et al. 2011. Microstructure and Mechanical Properties of Friction Stir Processed ODS Ferritic Steels. Journal of Nuclear Materials. 417: 245-248.

[26] Chen, Y.C., et al. 2012. Banded Structure and Its Distribution in Friction Stir Processing of 316L Austenitic Stainless Steel. Journal of Nuclear Materials. 420: 497-500.

[27] Yuan, W., et al. 2011. Effect of Texture on the Mechanical Behavior of Ultrafine Grained Magnesium Alloy. Scripta Materialia. 64: 580-583.

[28] Grewal, H.S., et al. 2013. Surface Modification of Hydroturbine Steel Using Friction Stir Processing. Applied Surface Science. 268: 547-555.

[29] Dodds, S., Jones, A.H. and Cater, S. 2013. Tribological Enhancement of AISI 420 Martensitic Stainless Steel Through Friction-Stir Processing. Wear. 302: 863-877.

[30] Cavaliere, P. and De Marco, P.P. 2007. Friction Stir Processing of AM60B Magnesium Alloy Sheets. Materials Science and Engineering A. 462: 393-397.

[31] Darras, B.M., et al. 2007. Friction Stir Processing of Commercial AZ31 Magnesium Alloy. Journal of Materials Processing Technology. 191: 77-81.

[32] Woo, W., et al. 2008. Microstructure, Texture and Residual Stress in a Friction-Stir-Processed AZ31B Magnesium Alloy. Acta Materialia. 56: 1701-1711.

[33] Du, X. and Wu, B. 2008. Using Friction Stir Processing to Produce Ultrafine-Grained Microstructure in AZ61 Magnesium Alloy. Transactions of Nonferrous Metals Society of China. 18: 562-565.

[34] Robson, J.D., Cui, S.and Chen, Z.W. 2010. Incipient melting During Friction Stir Processing of AZ91 Magnesium Castings. Materials Science and Engineering A. 527: 7299-7304.

[35] Yu, Z., et al. 2010. Influence of Thermo-Mechanical Parameters on Texture and Tensile Behavior of Friction Stir Processed Mg Alloy. Scripta Materialia. 63: 1112-1115.

[36] Yuvan, W., et al. 2011. Effect of Texture on the Mechanical Behavior of Ultrafine Grained Magnesium Alloy. Scripta Materialia. 64: 580-583.

[37] Mansoor, B. and. Ghosh, A.K. 2012. Microstructure and Tensile Behavior of a Friction Stir Processed Magnesium Alloy. Acta Materialia. 60: 5079-5088.

[38] Darras, B. and Kishta, E. 2013. Submerged Friction Stir Processing of AZ31 Magnesium Alloy. Materials and Design. 47: 133-137.

[39] Woo, W., et al. 2007. Influence of the Tool Pin and Shoulder on Microstructure and Natural Aging Kinetics in a Friction-Stir-Processed 6061-T6 Aluminum Alloy. Metallurgical and Materials Transactions A. 38: 69-76.

[40] Dolatkhah, A., et al. 2012. Investigating Effects of Process Parameters on Microstructural and Mechanical Properties of Al5052-SiC Metal Matrix Composite Fabricated via Friction Stir Processing. Materials and Design. 37: 458-464.

[41] Qu, J., et al. 2011. Improving the Tribological Characteristics of Aluminum 6061 Alloy by Surface Compositing with Sub-Micro-Size Ceramic Particles via Friction Stir Processing. Wear. 271: 1940-1945.

[42] Mishra, R.S., Ma, Z.Y. and Charit, I. 2003. Friction Stir Processing: a Novel Technique for Fabrication of Surface Composite. Materials Science and Engineering A. 341: 307-310.

[43] Fernandez, G.J. and Murr, L.E. 2004. Characterization of Tool Wear and Weld Optimization in the Friction-Stir Welding of Cast Aluminum 359+20% SiC Metal-Matrix Composite. Materials Chracterization. 52: 65-75.

[44] Tewari, A., et al. 2006. Characterization of the Effects of Friction Stir Processing on Microstructural Changes in DRA Composites. Materials Science and Engineering A. 428: 80-90.

[45] Mahmoud, E.R.I., Ikeuchi, K.and Takahashi, M. 2008. Fabrication of SiC Particle Reinforced Composite on Aluminium Surface by Friction Stir Processing. Science and Technology of Welding and Joining. 13: 607-618.

[46] Wang, W., et al. 2009. a Novel Way to Produce Bulk SiCp Reinforced Aluminum Metal Matrix Composites by Friction Stir Processing. Journal of Materials Processing Technology. 209: 2099-2103.

[47] Salehi, M., Saadatmand, M. and Aghazadeh Mohandesi, J. 2012. Optimization of Process Parameters for Producing AA6061SiC Nanocomposites by Friction Stir Processing. Transactions of Nonferrous Metals Society of China. 22: 1055-1063.

[48] Soleymani, S., Abdollah-zadeh, A. and Alidokht, S.A. 2012. Microstructural and Tribological Properties of Al5083 Based Surface Hybrid Composite Produced by Friction Stir Processing. Wear. 278-279: 41-47.

[49] Devaraju, A., Kumar, A. and Kotiveerachari, B. 2013. Influence of Rotational Speed and Reinforcements on Wear and Mechanical Properties of Aluminum Hybrid Composites via Friction Stir Processing. Materials and Design. 45: 576-585.

[50] Shafiei-Zarghani, A., Kashani-Bozorg, S.F. and Zarei-Hanzaki, A. 2009. Microstructures and Mechanical Properties of Al/Al2O3 Surface Nano-Composite Layer Produced by Friction Stir Processing. Materials Science and Engineering A. 500: 84-91.

[51] Zahmatkesh, B. and Enayazti, M.H. 2010. a Novel Approach for Development of Surface Nanocomposite by Friction Stir Processing. Materials Science and Engineering A. 527: 6734-6740.

[52] Mazaheri, Y., Karimzadeh, F. and Enayati, M.H. 2011. a Novel Technique for Development of A356/Al2O3 Surface Nanocomposite by Friction Stir Processing. Journal of Materials Processing Technology. 211: 1614-1619.

[53] Shariftabar, M., et al. 2011. Fabrication of 5052Al/Al2O3 Nanoceramic Particle Reinforced Composite via Friction Stir Processing Route. Materials and Design. 32: 4164-4172.

[54] Raaft, M., et al. 2011. Microstructural, Mechanical and Wear Behavior of A390/Graphite and A390/Al2O3 Surface Composites Fabricated Using FSP. Materials Science and Engineering A. 528: 5741-5746.

[55] Kashani-Bozorg, S.F. and Jazayeri, K. 2009. Formation of Al/B4C Surface Nano-Composite Layers on 7075 Al Alloy Employing Friction Stir Processing. AIP Conference Proceedings. 715: 1136-1140.

[56] Rejil, C.M., et al. 2012. Microstructure and Sliding Wear Behavior of AA6360/(TiC + B4C) Hybrid Surface Composite Layer Synthesized by Friction Stir Processing on Aluminum Substrate. Materials Science and Engineering A. 522: 336-344.

[57] Komarasamy, M., et al. 2013. Processing, Microstructure and Mechanical Property Correlation in Al-B4C Surface Composite Produced via Friction Stir Processing. in Friction Stir Welding and Processing VII. San Antonio.

[58] Bisadi, H. and Abasi, A. 2011. Fabrication of Al7075/TiB2 Surface Composite Via Friction Stir Processing. American Journal of Materials Science. 1: 67-70.

[59] Izadi, H. and Gerlich, A.P. 2012. Distribution and Stability of Carbon Nanotubes During Multi-Pass Friction Stir Processing of Carbon Nanotube/Aluminum Composites. Carbon. 50: 4744-4749.

[60] Ma, Z.Y., et al. 2013. Fabrication of Carbon Nanotube Reinforced Aluminum Matrix Composites via Friction Stir Processing. in Friction Stir Welding and Processing VII. San Antonio.

[61] Liu, Q., et al. 2013. Microstructure and Mechanical Property of Multi-Walled Carbon Nanotubes Reinforced Aluminum Matrix Composites Fabricated by Friction Stir Processing. Materials and Design. 45: 343-348.